Supplementary information

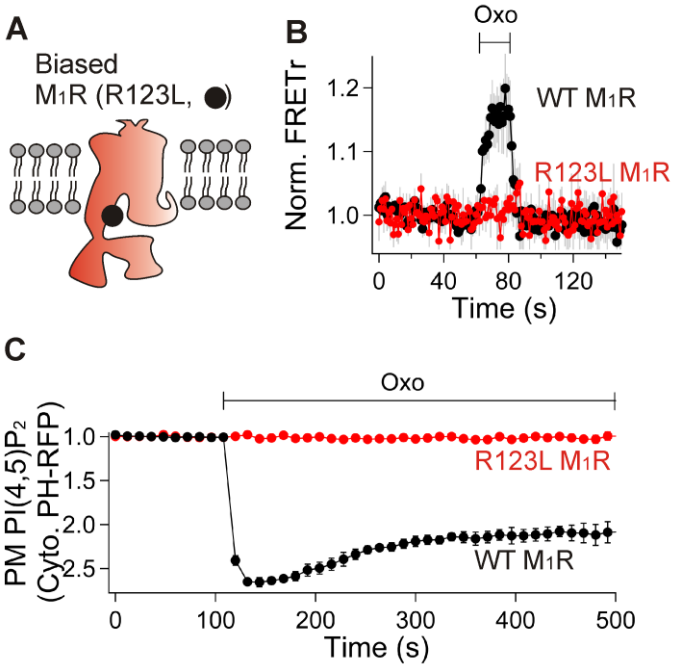

Fig. S1. Absence of G-protein coupling to β-arrestin biased M_1R (R123L M_1R). (A) Schematic diagram of the arginine (R) to leucine (L) mutation in the third transmembrane domain (black circle). (B) FRETr interaction between G_q-CFP and R123L M_1R-SNAP505 (red) compared to WT M_1R-SNAP505 (black). N = 5. (C) $PI(4,5)P_2$ hydrolysis monitored with the $PI(4,5)P_2$-sensitive PH-RFP probe in confocal microscopy (see Materials and Methods). The y-axis for the normalized cytosolic intensity of PH-RFP probe is inverted to reflect $PI(4,5)P_2$ depletion at the plasma membrane by WT M_1R (black symbols, N = 2, n = 4) or R123L M_1R (red symbols, N = 2, n = 6). Experiments for this figure used 100 µM oxotremorine (Oxo).

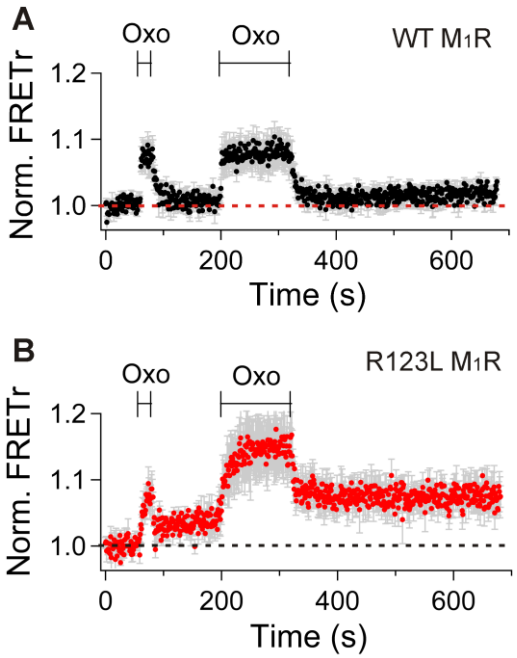

Fig. S2. Time-dependent formation of stable β-arrestin binding to M_1R. (A and B) Normalized intermolecular FRETr between β-arrestin 2 CFP and SNAP505-labeled WT M_1R (A, N = 5) or R123L M_1R (B, N = 3). Oxotremorine (Oxo) was applied first for 20 s and then for 2 min in sequence to the same cells in individual experiments. Dashed line indicates the basal level of normalized FRETr.

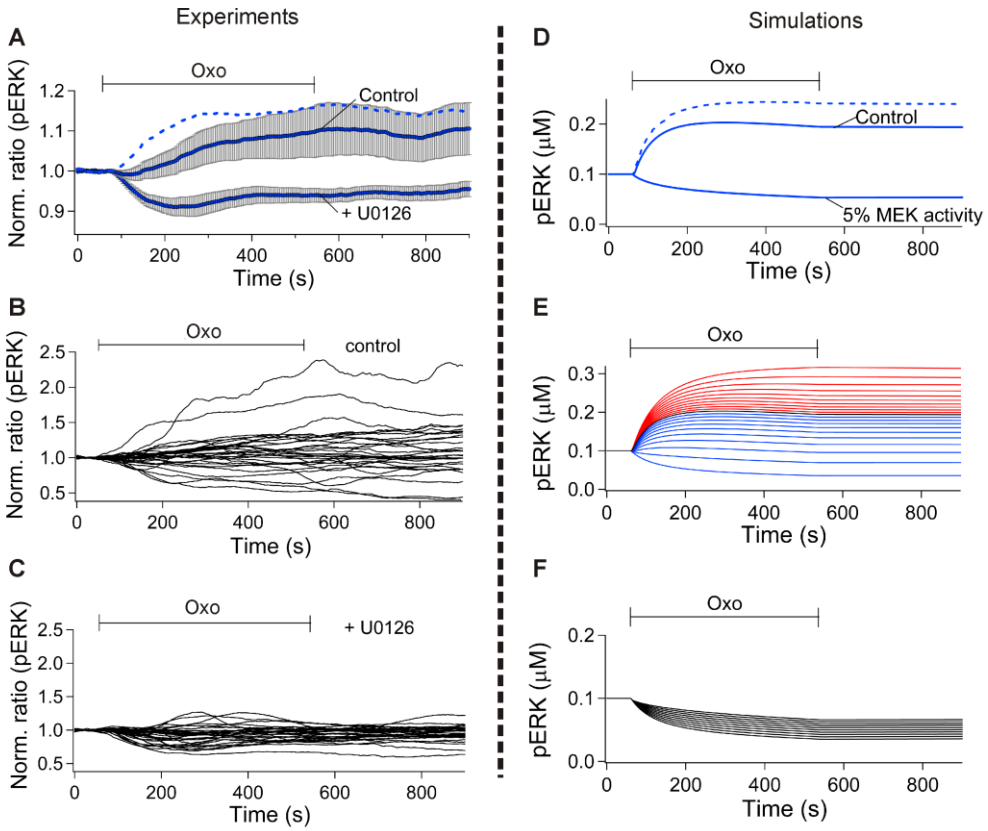

Fig. S3. ERK activation by the biased M_1R (R123L M_1R). Activated ERK (pERK) was measured as the ERK KTR ratio (I_{cyt}/I_{nuc}) and normalized to remove cell-to-cell variation (Norm. ratio). (A) Averaged time course of ERK KTR ratio after addition of oxotremorine (Oxo) without (Control) or with 3-min preincubation with 10 μM U0126, a MEK1/2 inhibitor (+ U0126). The dashed line is Control minus U0126. (B, C) Raw data for (A). Each trace is from a single cell without (B, N = 4, n = 34) or with (C, N = 4, n = 33) the inhibitor. (D-F) Simulation of ERK phosphorylation with our mathematical model (See Fig. 4D). (D) Simulated ERK phosphorylation with 100% (Control) or 5% of MEK activity. The 5% trace simulates block by the inhibitor. The dashed line shows Control minus the 5% MEK effect. (E) Simulation of cell-to-cell variability in rates. Individual lines represent single simulations with a progressive variation of the rate constants for MEK or protein phosphatase (Reactions 10 and 13 in Fig. 4D). For the blue lines, MEK activity was reduced stepwise by 10%. For the red lines, the phosphatase activity was reduced stepwise by 10%. The black line in the middle represents 100% activity for each and is identical to Control in D. (F) Simulations obtained by varying the rate constant for MEK (0 to 9% of maximum rate constant) at a fixed rate constant for protein phosphatase (100%). 100 μM Oxo was used for all experiments and simulations.

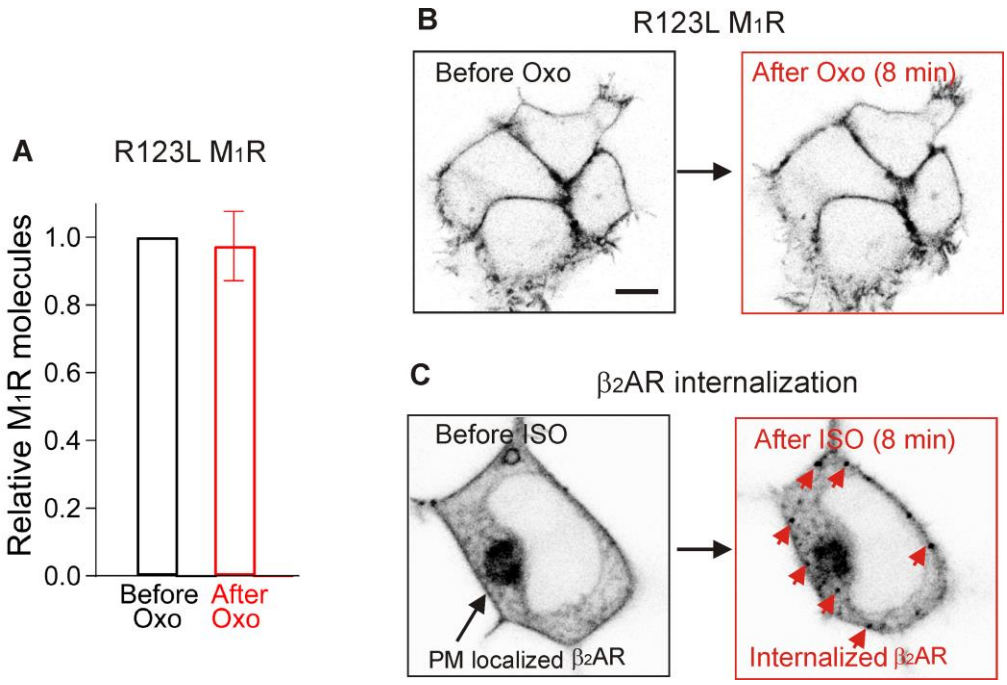

Fig. S4. Lack of internalization of activated R123L M_1R (biased M_1R). (A) Relative number of M_1R molecules at or near the plasma membrane before and after 8 min in 100 µM Oxo measured by single-molecule TIRF microscopy. N = 4. (B) Confocal images of R123L M_1R-SNAP647 before and after 8 min in 100 µM Oxo. (C) Confocal images for CFP tagged β_2-AR (β_2-adrenergic receptor) before and after 10 µM isoproterenol (ISO), a β_2-AR agonist. In contrast to M_1R, internalized β_2-ARs are visible in intracellular vesicles (arrow heads). Confocal images are inverted so that fluorescence signals appear black.

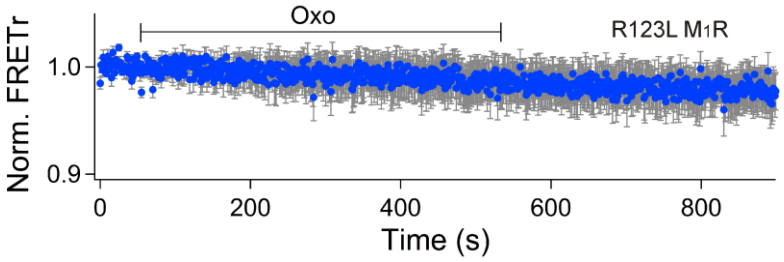

Fig. S5. No receptor-induced conformational change of β-arrestin when complexed with R123L M_1R. Intramolecular FRET was measured using FlAsH-tagged β-arrestin 2 CFP during application of 100 µM oxotremorine (Oxo). N = 9.

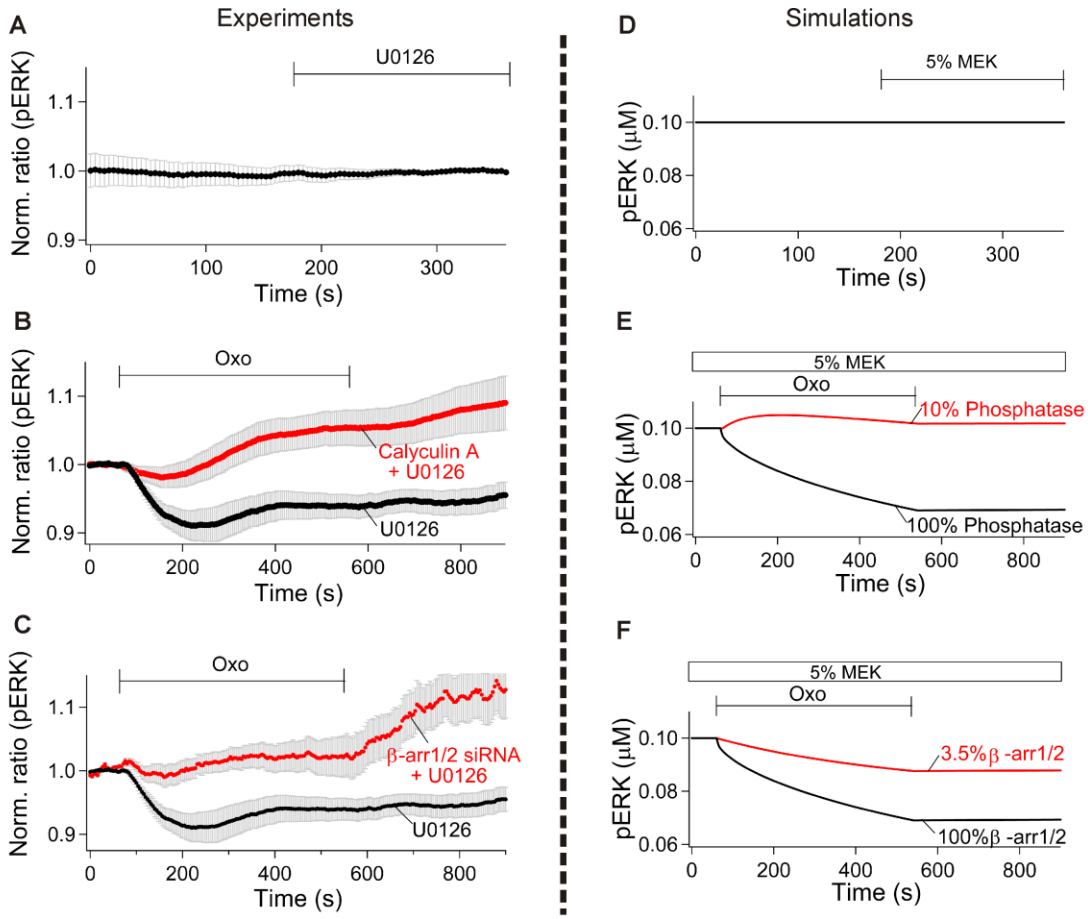

Fig. S6. Negative control of pERK by the biased M_1R involves β-arrestin and serine/threonine protein phosphatases. Plots show time course of the pERK KTR signal as a measure of activated ERK. (A) The MEK1/2 inhibitor (U0126) did not change the basal ERK activity signal, suggesting no basal activity of MEK1/2 (N = 4, n = 33). (B) After a 3-min pretreatment with the MEK inhibitor alone, the M_1R agonist (Oxo, 100 μM) reduced ERK activity (black, N = 4 and n = 33). Pretreatment with the PP1 and PP2A protein phosphatase inhibitor calyculin A (20 nM), antagonized the negative effect (red, N = 4, n = 28). The protein phosphatase inhibitor did not have any effect on the basal ERK KTR ratio, suggesting no basal activity of the protein phosphatases. (C) Knockdown of β-arrestin 1 and 2 using siRNA (red, N = 4, n = 31) had a similar effect on ERK activity as calyculin A. (D-F) Simulation of the effect of calyculin A and β-arrestin 1/2 knock-down on pERK. (D) The MEK inhibitor did not affect the basal pERK. For the simulation, MEK activity was reduced to 5% by the MEK inhibitor ('5% MEK', Reaction 10 in Fig. 4D). (E) To simulate the effect of calyculin A, the protein phosphatase was reduced to 10% by adjusting the rate constant of Reaction 13 in Fig. 4D. (F) For knock-down of β-arrestin 1/2 using siRNA, 96.5% of arrestin was assumed to be removed ('3.5% β-arr1/2'). 100 μM Oxo was used in all experiments and simulations.

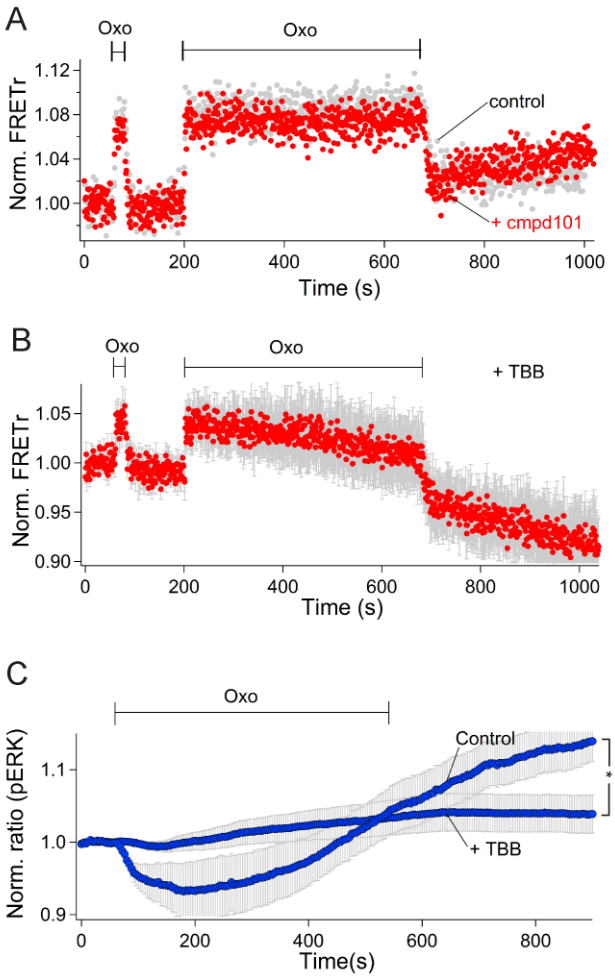

Fig. S7. Stabilization of β-arrestin and ERK activity with WT M_1R was regulated by CK2 but not by GRK2/3 protein kinases. (A) Intermolecular FRET measured between β-arrestin 2 and WT M_1R. Oxotremorine (Oxo) was applied for 20 s in the first pulse and then washed off. The same cells were treated with Oxo for 8 min. The red symbols indicate cells pretreated with 30 μM cmpd101 for 3 min and the blocker was present during the whole experiment (N = 5). The gray symbols are obtained from the control cells without the GRK2/3 blocker (from Fig. 2B). Error bars are omitted for clarity. (B and C) A selective inhibitor of CK2, TBB (10 μM), significantly blocked the persistent level of intermolecular FRET (B, N = 6) and ERK activity (C, N = 4, n = 29, P = 0.03 (*)) with WT-M_1R. The cells were pretreated with the inhibitor for at least 3 min before addition of Oxo and then Oxo was added for additional 8 min in the presence of the blocker. The control trace for ERK activity was obtained from Fig. 3H. 100 μM Oxo was used for all experiments.

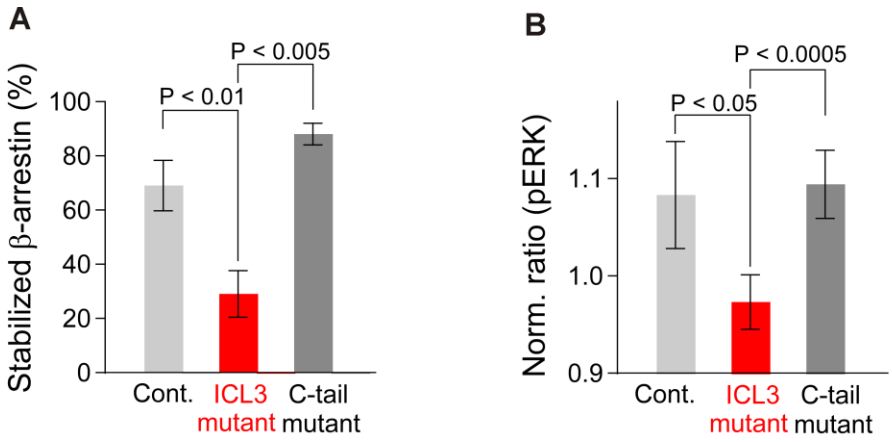

Fig. S8. Formation of stable β-arrestin-receptor complexes and activation of ERK by different mutants of R123L M_1R (biased M_1R). The percentage of stabilized β-arrestin measured with intermolecular FRETr (A) and ERK activity (B) after washing off M_1R agonist. After application of oxotremorine (Oxo) for 8 min, we estimated sustained levels during the following 6 min without the agonist. Light gray, red, dark gray bars indicate control, alanine mutant at two serine sites (S228A and S273A) in the third intracellular loop (ICL3 mutant), and alanine mutant at S451 and S457 in the C-tail of C-terminus (C-tail mutant), respectively. (A) Control (N = 9), ICL mutant (N = 4), and C-tail mutant (N = 5). (B) Control (N = 4, n = 34), ICL3 mutant (N = 4, n = 52), and C-tail mutant (N = 4, n = 52). The parameters were not significantly different between control and C-tail mutant. 100 μM Oxo was used for these experiments.

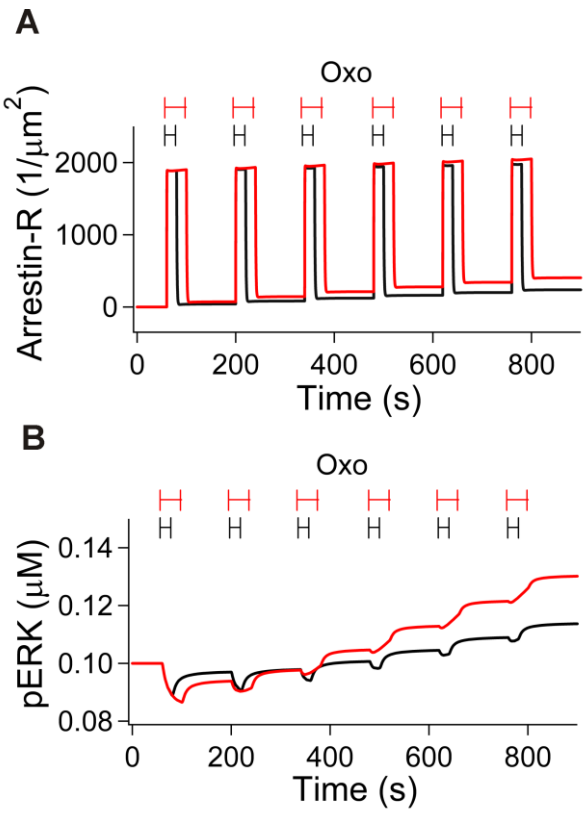

Fig. S9. Simulation of gradual rise of stably bound arrestin during repetitive stimulations of WT M_1R. Total number of arrestin-bound receptor (A) and ERK phosphorylation (B) in repetitive applications of agonist (Oxo) in 20 s (black) and 40 s (red) duration. 100 μM Oxo was used for these simulations.

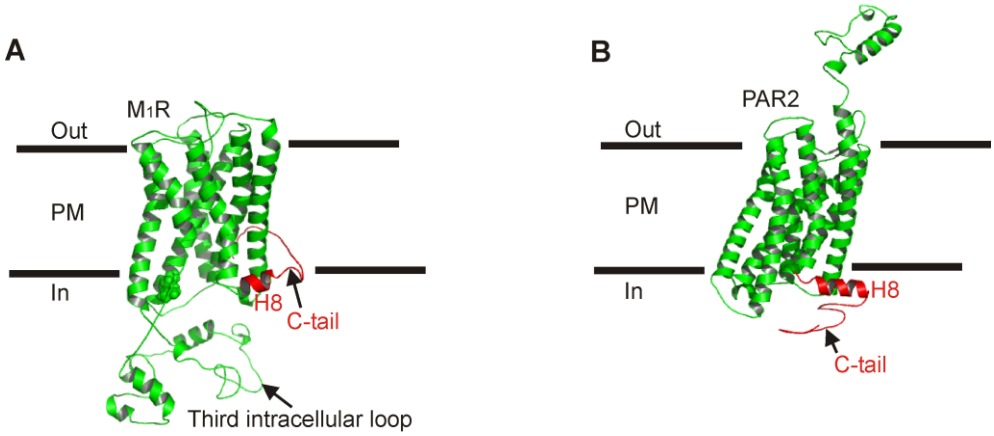

Fig. S10. Simulation of mouse M_1R and human PAR2 structures. The whole structures of M_1R (A) and PAR2 (B) were simulated with I-TASSER. The C-tail of each receptor is highlighted in red. The C-tail of M_1R extending from helix 8 (H8) was not well positioned to the cytosolic interface to interact with arrestin partly because of occlusion by the extensive intracellular loop, while that of PAR2 is well exposed for arrestin binding. See Materials and Methods for detailed description about this simulation.

Table S1

Model initial conditions and parameters

Species/rate constants	Value	Rationale
R (Receptor)	3,500 μm^{-2}	Receptor density at the plasma membrane (reference 1, Jung et al., 2016)
β-arrestin	15 μM	Cytosolic concentration of arrestins. We did not distinguish between β-arrestin 1 and 2 (reference 1, Jung et al., 2016).
GRK	1000 molecules$*\mu m^{-2}$ (if it is completely dissolved in cytosol, it would be 0.5 μM)	Membrane localized GRK pool for biased M_1R. For WT M_1R, we assumed that the GRK pool was only 1% left because of depletion of PI(4)P and $PI(4,5)P_2$.
CK2	5 μM	Cytosolic concentration of CK2 for WT M_1R modeling. No CK2 action in the biased receptor model.
MEK	1 μM	Cytosolic MEK concentration (reference 2, Fujioka et al., 2006). To reduce unknown free parameters, we did not add the step for phosphorylation of MEK by the c-Raf. If MEK binds to the arrestin-GPCR complex, it can phosphorylate the ERK at the plasma membrane.
ERK	1 μM	Cytosolic ERK concentration (reference 2, Fujioka et al., 2006).
pERK	100 nM	Basal level of phosphorylated ERK concentration. We assumed that 10% of total ERK was phosphorylated before M_1R activation.
PM	886 μm^2	Total area of the plasma membrane
Cytosol	2,500 μm^3	Total volume of the cytosol
EC	250,000 μm^3	Extracellular volume for simulation
Protein phosphatase (PP)	5 μM	Fitted to our pERK data.
$k_{1,f}$	20 $s^{-1}*\mu M^{-1}$	Binding rate constant of ligand to R
$k_{1,r}$	4 s^{-1}	Dissociation rate constant of ligand from R to match for K_d of Oxo (~ 0.2 μM)
$k_{2,f}$	0.28 $s^{-1}*\mu M^{-1}$	Rate constant for binding of β-arrestin to RL (ligand-bound R)
$K_{2,r}$	2.4 s^{-1}	Rate constant for dissociation of β-arrestin to RL
$K_{3,f}$	4 $\mu m^2*s^{-1}*molecules^{-1}$	Rate constant for binding of GRK
	(0.00005 $s^{-1}*\mu M^{-1}$)	(Rate constant for binding of CK2)
$k_{3,r}$	4 s^{-1}	Rate constant for dissociation of GRK
	(1 s^{-1})	(Rate constant for dissociation of CK2)
$k_{4,f}$	0.9 s^{-1}	Rate constant for phosphorylation at both of S228 and S273 of RL by GRK (or CK2)
	(0.01 s^{-1})	

$K_{5,f}$	2 s^{-1} (10 s^{-1})	Rate constant for dissociation of GRK after phosphorylation (Rate constant for dissociation of CK2 after phosphorylation)
$k_{5,r}$	100 $\mu m^2 * s^{-1} * molecules^{-1}$ (10 $s^{-1} * \mu M^{-1}$)	Rate constant for rebinding of GRK (or CK2) to phosphorylated receptor (RLpp)
k_6	0.5 s^{-1}	Rate constant for dephosphorylation of phosphorylated receptor (RLpp) by nonspecific protein phosphatase
$k_{7,f}$	1 $s^{-1} * \mu M^{-1}$	Rate constant for β-arrestin binding to phosphorylated M_1R at both of S228 and S273
$k_{7,r}$	10 s^{-1}	Rate constant for β-arrestin dissociation from phosphorylated M_1R at both of S228 and S273 (RLpp)
$k_{8,f}$	0.1 $s^{-1} * \mu M^{-1}$	Rate constant for MEK binding to RLppA
$k_{8,r}$	0.00005 s^{-1}	Rate constant for MEK dissociation from RLppAM
$k_{9,f}$	0.5 $s^{-1} * \mu M^{-1}$	Rate constant for ERK binding to RLppAM
$k_{9,r}$	2.5 s^{-1}	Rate constant for ERK dissociation from RLppAME
$k_{10,f}$	3 s^{-1} (9 s^{-1})	Rate constant for phosphorylation of ERK (RLppAME) by MEK in biased receptor (or WT M_1R)
$k_{10,r}$	0.03 s^{-1} (0.36 s^{-1})	Rate constant for dephosphorylation of pERK (RLppAMpE) by nonspecific protein phosphatases to make steady-state of pERK in biased receptor (or WT M_1R)
k_{11}	2 s^{-1}	Rate constant for dissociation of pERK from RLppAMpE
$k_{12,f}$	0.0001 $s^{-1} * \mu M^{-1}$ (0.00003 $s^{-1} * \mu M^{-1}$)	Rate constant for binding of protein phosphatase (PP) to RLA in biased receptor (or WT M_1R)
$k_{12,r}$	0.00006 s^{-1}	Rate constant for dissociation of protein phosphatase (PP) from RLAPP
k_{13}	24 $s^{-1} * \mu M^{-1}$ (90 $s^{-1} * \mu M^{-1}$)	Rate constant for dephosphorylation of pERK by RLAPP in biased receptor (or WT M_1R)

Reference

1 Jung SR, et al (2016) Contributions of protein kinases and β-arrestin to termination of protease-activated receptor 2 signaling. *J Gen Physiol* 147:255-271.

2 Fujioka A, et al (2006) Dynamics of the Ras/ERK MAPK cascade as monitored by fluorescent probes. *J Biol Chem* 281:8917-8926.